ACS OMEGA

http://pubs.acs.org/journal/acsodf

Article

# Optical, Structural, and Magnetic Hyperthermia Properties of Yttrium Iron Garnet Synthesized by Hybrid Microwave-Assisted Hydrothermal and Sol–Gel Auto Combustion Routes

Basil Chacko, Avanish Babu Thirumalasetty, Vembakam Vijayakanth, and Madhuri Wuppulluri*

Cite This: *ACS Omega* 2023, 8, 19367–19373

Read Online

ACCESS | Metrics & More | Article Recommendations | Supporting Information

**ABSTRACT:** Magnetic hyperthermia is an emerging technique used for the treatment of tumors, where the infected cells will be deactivated using the heat generated from magnetic particles. This study discusses the viability of yttrium iron garnet (YIG) in magnetic hyperthermia treatment. YIG is synthesized using hybrid microwave-assisted hydrothermal and sol–gel auto combustion techniques. The formation of the garnet phase is confirmed using powder X-ray diffraction studies. Further, the morphology and grain size of the material are analyzed and estimated with the help of field emission scanning electron microscopy. Transmittance and optical band gap are obtained using UV–visible spectroscopy. Raman scattering of the material is discussed to understand the phase and vibrational modes. The functional groups of garnet are studied using Fourier transform infrared spectroscopy. Further, the effect of the synthesizing routes on the characteristics of the materials is discussed. A relatively higher magnetic saturation value is observed in the hysteresis loop at room temperature of YIG samples, which is synthesized by a sol–gel auto combustion technique, and it confirms the ferromagnetic behavior. The colloidal stability and surface charge of the prepared YIG are evaluated by a zeta potential measurement. In addition, magnetic induction heating studies are carried out for both prepared samples. The specific absorption rates of 1 mg/mL concentration are 237 and 214 W/g at 35.33 kA/m and 316 kHz field of sol–gel auto combustion and hydrothermal methods, respectively. Due to their higher saturation magnetization of 26.39 emu/g, the sol–gel auto combustion method produced effective YIG and demonstrated superior heating efficiency than the hydrothermally prepared sample. The prepared YIG are biocompatible, and their hyperthermia properties may be explored in various biomedical applications.

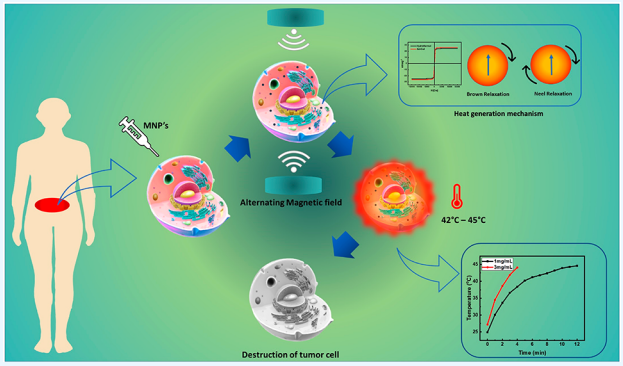


## 1. INTRODUCTION

Yttrium iron garnet (YIG) is a cubic crystal and belongs to the space group Ia3d. It contains eight formula units per unit cell and is chemically represented as $Y_3Fe_5O_{12}$.[1] In YIG, $Y^{3+}$ atoms occupy the 24c (dodecahedral) sites, $Fe^{2+}$ atoms occupy the 16a (octahedral) sites, and $Fe^{3+}$ atoms occupy the 24d (tetragonal) sites, which are formed by the surrounding $O^{2-}$ ions.[2] The orientation of the magnetic moments of iron ions is where YIG gets its essential magnetic characteristics. The magnetic moments of two octahedrally positioned $Fe^{3+}$ ions are oriented antiparallel to those of three tetrahedrally positioned $Fe^{3+}$ ions. On the other hand, the dodecahedral site is where nonmagnetic $Y^{3+}$ ions should be located. Due to the interaction of nearby oxygen ($O_2$) ions, the $Fe^{3+}$ ions at the octahedral (a) and tetrahedral (d) sites contribute most to the effective magnetic moment.[3] YIG belongs to a significant class of magnetic oxides with a wide range of applications attributed to its properties, such as its high melting point, thermal stability, chemical stability, thermal conductivity, large resistivity, and low thermal expansion. In view of its diverse properties, YIG nanoparticles (NPs) are the best suitable materials for a wide variety of applications in electromagnetic, microwave, and magneto-optic devices. Also, it has been widely used in biomedical applications such as magnetic resonance imaging contrast agents for cancer tumor detection, hyperthermia, drug delivery, selective separation, and biomolecule detection.[4]

As the current cancer treatment techniques have side effects and limitations, the dramatic increase in the number of people affected by cancer has raised serious concerns in the research field about finding better alternatives for cancer treatment. Research is going on to find alternatives where cancer cells can be effectively eliminated with minimal damage or without

Received: January 10, 2023
Accepted: April 6, 2023
Published: May 22, 2023

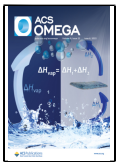

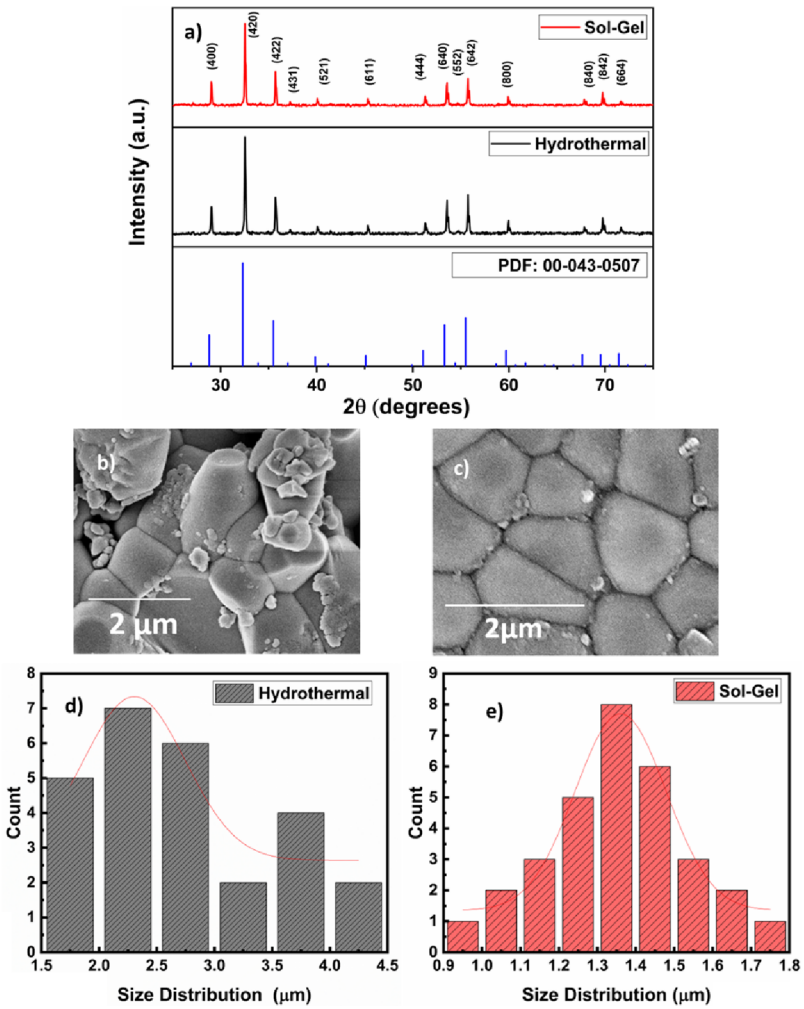


**Figure 1.** (a) XRD pattern, (b, c) FESEM images, and (d, e) size distribution histogram of YIG synthesized by hydrothermal and sol−gel auto combustion methods.

causing any damage to the healthy cells.[5] Excellent magnetic characteristics have been demonstrated by iron oxide-based NPs, which have been widely employed in magnetic hyperthermia applications for cancer treatment.[5] Iron oxide crystals can alter their magnetic characteristics as a result of incorporating foreign atoms, making them ideal for hyperthermia applications.[6] Iron oxides undergo magnetic transitions due to rare earth metals, which lowers the Curie transition temperature.[7] Hyperthermia is a significant technique used in the treatment of cancer.[8] There are various types of hyperthermia, which are mainly divided into local hyperthermia (MH), whole-body hyperthermia, and regional hyperthermia.[9] The magnetic hyperthermia gives the SHGR (specific heat generation rate) value, which is an important parameter for determining the dosage and duration of treatment.[10] The body temperature affects our basic metabolism.[11] With respect to normal body temperature, at low-temperature ranges, there is an exponential increase in biochemical reaction rates.[12] An increase in the rate of biochemical reactions and activity of the enzymes are observed in higher temperatures. Enzymes start to break down at a temperature above 40 °C.[13] Thus, a body temperature range of 40 to 44 °C is said to be cytotoxic for normal cells and is called hyperthermia.[14] These studies reveal that hyperthermia therapy can be used as an independent therapy, similar to industry standard radiation therapy, chemotherapy, and immunotherapy for cancer treatment.[15,16] In conventional whole-body hyperthermia and regional hyperthermia techniques (ultrasonic, capacitive, and inductive techniques), the body around the tumor is used to heat and this heating is nonhomogeneous.[14] The precision and efficiency of hyperthermia treatment can be increased by a localized heating.[17] This can be facilitated with the help of magnetic hyperthermia and nanotechnology.[14] Magnetic hyperthermia can be obtained by introducing magnetic materials under alternating magnetic field. Various phenomena such as eddy current heating, magnetic hysteresis loss, and magnetic moment relaxation are responsible for magnetic hyperthermia.[18]

Magnetic hyperthermia properties of YIG synthesized using hydrothermal and sol−gel auto combustion techniques are studied. Chemical synthesis approaches have an advantage over physical methods because they require low temperatures for sintering, produce fine NPs, are quick and easy while synthesizing, produce a uniform morphology, are inexpensive to use, remain chemically stable, and have a high reproducibility rate.[19] The synthesized materials are systematically evaluated and reported.



https://doi.org/10.1021/acsomega.3c00162
ACS Omega 2023, 8, 19367−19373

## 2. EXPERIMENTAL DETAILS

YIG is synthesized using sol−gel auto combustion and hydrothermal methods. In the hydrothermal method, the precursors used for the hydrothermal method are yttrium oxide [$Y_2O_3$] (99.99%, Sigma-Aldrich, India), nitric acid [$HNO_3$] (70%, Sigma-Aldrich, India), and ferric nitrate [$Fe(NO_3)_3 \cdot 9H_2O$] (98%, Merck, India). The precursors are taken in stoichiometric ratios and dissolved in double-distilled water by continuous stirring. Ammonium hydroxide is added to the solution for maintaining a pH of 11. Maintaining a pH of 11 will help complete the formation of nanoferrite precipitates in an autoclave.[20] After maintaining the pH of 11, the solution is stirred continuously for another 2 h, which results in the formation of a homogeneous solution and initiates the reaction. Further, the solution is transferred to a 300 mL Teflon-lined, sealed autoclave and is heat-treated at 195 °C for 7 h in a hot air oven. After 7 h, the sealed autoclave was slowly brought down to room temperature. The product obtained is filtered and washed with distilled water until the pH reaches 7. The obtained product is dried at 60 °C for another 8 h. The sample is grinded to fine particles using an agitate mortar and pressed into pellets using a hydraulic press. The pellets are preheated at 1000 °C for 30 min using a microwave-programmable furnace fitted with dual magnetrons, operating at a frequency of 2.45 GHz. A schematic diagram of the synthesis technique is given in Figure S1. The pellet obtained is once again milled and pressed into pellets and sintered at 1250 °C for another 30 min using the microwave furnace. Microwave heating allows for rapid phase formation and accelerates elemental diffusion in the precursor powder, resulting in the rapid formation of the YIG phase while preserving the nanostructure.[21]

Yttrium oxide [$Y_2O_3$] (99.99%, Sigma-Aldrich, India), nitric acid [$HNO_3$] (70%, Sigma-Aldrich, India), and ferric nitrate [$Fe(NO_3)_3 \cdot 9H_2O$] (98%, Merck, India) are the precursors used in the synthesis of YIG by the sol−gel auto combustion technique. The precursors are taken in a stoichiometric ratio and dissolved in a minimal amount of double-distilled water. The solution is stirred for 30 min at 80 °C. Citric acid is added to the prepared solution as a fuel agent. The pH of the mixture is kept at 7 by gradually adding ammonia solution. To maintain the ambient temperature, the mixture is kept in a water bath while adding the ammonia solution. After maintaining pH at 7, the mixture is stirred vigorously at 90 °C until the solution gets evaporated to 1/3 of the initial amount of solution. Ethylene glycol is added to the solution to enhance the reaction and gel formation. Adding ethylene glycol will also reduce the agglomeration of particles. The mixture is heated to 120 °C until it gels and burns down to powder. Using a hydraulic press, the powder is formed into pellets. The samples are presintered in the microwave furnace for 30 min at 1000 °C. The presintering ensures the evaporation of unwanted organic elements and formation of oxides. The obtained sample is once again milled and pressed into pellets. The sample is sintered at 1250 °C for 30 min in the microwave furnace. A schematic diagram of the synthesis technique is given in Figure S2.

The sintered samples are used to study the various properties. The structural properties are analyzed using a Bruker D8 X-ray diffractometer. The morphology and elemental composition are observed using a Carl Zeiss EVO 18 Research scanning electron microscope. The optical properties are studied using a UV−visible spectrophotometer, JASCO (V-670 PC), and Raman spectroscopy (= 536 nm), Agiltron. Functional groups are studied using an IRAffinity-1, Shimadzu, FTIR photo spectrometer. Magnetic properties are studied from a vibrating sample magnetometer (Lake Shore) and hyperthermia biomedical applications using an Ambrell (EASYHEAT, UK) induction system (8310 LI).

## 3. RESULTS AND DISCUSSION

**3.1. Structural Analysis.** The X-ray diffraction (XRD) technique is used to analyze the structural properties of nanostructures. Figure 1a shows the room-temperature XRD pattern of YIG synthesized by both hydrothermal and sol−gel auto combustion techniques in the $2\theta$ range from 20 to 80°. It is found that YIG has a cubic structure with the space group Ia3d.[22] The XRD peaks confirm the garnet phase formation and exhibit good crystalline phases for YIG in both the samples. The peaks are observed at (400), (420), (422), (431), (521), (611), (444), (640), (552), (642), (800), (840), (842), and (664) and are matched with JCPDS file no. 00-043-0507.

Table 1 shows the various structural parameters determined from XRD. The crystallite size is calculated using the Scherrer formula.[23] Further, the strain,[24] dislocation density, lattice parameter,[25] and density[26] of the samples are shown in Table 1.

**Table 1. Structural Parameters of YIG from XRD**

| structural parameters | synthesis technique | |
|---|---|---|
| | hydrothermal | sol−gel auto combustion |
| crystallite size $D$ (nm) (∼±0.01%) | 59.95 | 56.45 |
| strain $\varepsilon$ ($\times 10^{-3}$) (∼±0.01%) | 2.1 | 2.0 |
| dislocation density $\delta$ ($\times 10^{14}$) ($cm^{-2}$) (∼±0.01%) | 2.78 | 3.13 |
| lattice parameter $a$ (nm) (∼±0.8%) | 1.22 | 1.22 |
| theoretical density ($gcm^3$) (∼±0.9%) | 5.22 | 5.22 |

**3.2. Morphological Analysis.** Figure 1b,c shows the morphology of the microwave-sintered $Y_3Fe_5O_{12}$ by hydrothermal and sol−gel auto combustion methods. A uniform grain growth is observed in both the cases. A smaller grain size is observed in YIG synthesized by a sol−gel auto combustion mechanism. Also, the smaller grains are attributed to the microwave sintering. The average grain size from FESEM images is calculated using ImageJ software and the histogram of size distribution is plotted in Figure 1d,e. It is observed to be 2.3 and 1.36 $\mu$m for YIG synthesized by hydrothermal and sol−gel auto combustion techniques, respectively.

Energy-dispersive X-ray (EDX) microanalysis is an elemental evaluation approach associated to SEM. Based on the generation of representative X-rays, elemental composition present in the target material can be mapped.[27] Figure S3 depicts the EDX spectra of YIG synthesized via hydrothermal and sol−gel auto combustion methods. It represents the peaks of yttrium, iron, and oxygen. No impurity peaks are observed in the EDX spectra.

**3.3. Optical Properties.** *3.3.1. UV−Visible Spectroscopy.* The transmission spectra of synthesized YIG by hydrothermal and sol−gel auto combustion methods are shown in Figure S4. The material is found to be highly transparent deep in the UV region (<1000 nm).

The optical band gap for synthesized YIG is determined using Tauc's relation.[28]



https://doi.org/10.1021/acsomega.3c00162
ACS Omega 2023, 8, 19367−19373

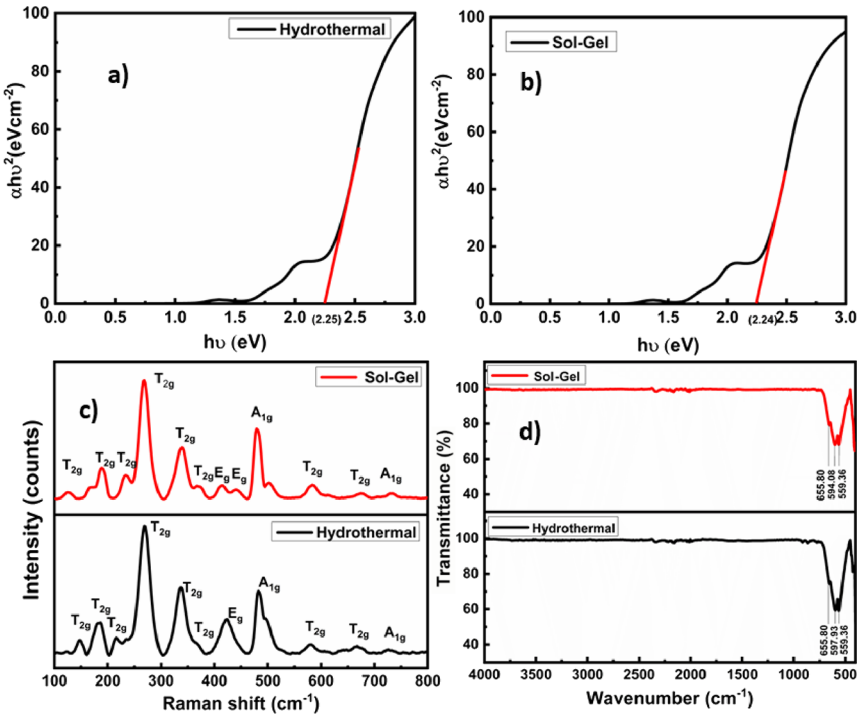


**Figure 2.** (a, b) Tauc's plot, (c) Raman spectroscopy, and (d) FTIR spectroscopy of YIG in hydrothermal and sol−gel auto combustion methods.

The band gap values are determined, assuming the direct band gap, as shown in Figure 2a,b. It is observed that there are no significant changes in the optical band gap while synthesizing YIG in hydrothermal and sol−gel auto combustion methods.

*3.3.2. Raman Spectroscopy.* Figure 2c shows the Raman spectroscopy of YIG synthesized through hydrothermal and sol−gel auto combustion methods, followed by microwave sintering at 1250 °C. The bcc unit cell of YIG is having 160 atoms inside and group theory suggests that there should be $3A_{1g} + 8E_g + 14T_{2g}$ modes in the first-order Raman spectrum.[29] The crystallographic sites of the garnet structure are correlated with the vibrational activity of the 25 Raman phonons of YIG.[30] Eleven and twelve out of the 25 Raman-active modes have been measured in hydrothermal and sol−gel auto combustion methods, respectively. In this regard, some modes may not be detected as they are too weak, and there may also be inadvertent degeneracy of discrete modes at atmospheric pressure.[31] The $Fe^{3+}$ ions situated within the octahedral (16a) sites have no effect on YIG's Raman activity.[30] The $Y^{3+}$ ions within the dodecahedral sites (24c) have $E_g + 2T_{2g}$ irreducible representations, $Fe^{3+}$ ions within the tetrahedral sites (24d) have $E_g + 3T_{2g}$ irreducible representations, while the $O^{2-}$ ion (96h) sites have $3A_{1g} + 6E_g + 3T_{2g}$ irreducible representations. The lattice or exterior modes of the polyhedral units are allocated to the $E_g$ and $T_{2g}$ bands located under 300 $cm^{-1}$, which are obtained from translations of the tetrahedral (24d) and dodecahedral (24c) units as well as vibrational motions of the $FeO_4$ tetrahedron.[32] The $T_{2g}$ mode at 268.47 $cm^{-1}$ is attributed to the translational vibration of the cations present in the tetrahedral and dodecahedral sites in the garnet crystal lattice.[31] The $T_{2g}$ vibration mode is more intense, which describes the pure garnet phase formation and follows the Franck−Condon principle, which asserts that, in an electronic transition, a shift from one vibrational energy level to another energy level has a higher probability if the two vibrational wave functions overlap.[33] Additionally, the Raman bands above 300 $cm^{-1}$ correspond to internal modes of the $Fe^{3+}$ polyhedra, and they are characterized by displacements of lighter oxygen ions.[30] The vibrational mode at ∼730 $cm^{-1}$ represents the $A_{1g}$ phonon and is assigned to the symmetrical stretching of the $FeO_4$ tetrahedron.[34,35]

**3.4. FTIR Analysis.** The determination of the garnet phase and analysis of the chemical bond are done by FTIR studies. For the synthesized YIG samples, the FTIR spectra are recorded in a frequency range of 400−4000 $cm^{-1}$. Figure 2d shows the FTIR spectra obtained for YIG synthesized by hydrothermal and sol−gel auto combustion methods. The formation of the garnet phase is represented by the absorption bands $v_1$ and $v_2$ present in the frequency range of 400 to 800 $cm^{-1}$. The FTIR results show strong absorption bands in the range of 500−700 $cm^{-1}$. The absorption band at 559.36 and 655.80 $cm^{-1}$ represents the asymmetric stretching at the tetrahedral site and octahedral site of metal ions and oxygen ions, respectively.[36]

**3.5. Magnetic Properties.** *3.5.1. VSM Analysis.* Figure 3a shows the magnetic hysteresis curve of YIG. The hysteresis loop measured at room temperature confirms its ferromagnetic nature. From the hysteresis, the saturation magnetization $M_s$ is 24.78 and 26.39 emu/g, the remnant magnetization $M_r$ is 0.147 and 0.145 emu/g, and the coercive field $H_c$ is 3.39 and 3.14 Oe for YIG synthesized by hydrothermal and sol−gel auto combustion methods, respectively. A very low coercive field indicates that the YIG synthesized is a soft ferrite. Table 2 presents the properties obtained from the hysteresis loop for YIG synthesized by various methods and compared with the present results. It is visible that compared to other synthesis techniques, the produced YIG has almost zero coercivity, remanent magnetization, and higher saturation magnetization values for both the samples prepared.

*3.5.2. Zeta Potential.* The zeta potential (ZP) of YIG synthesized by hydrothermal and sol−gel auto combustion


https://doi.org/10.1021/acsomega.3c00162
ACS Omega 2023, 8, 19367−19373

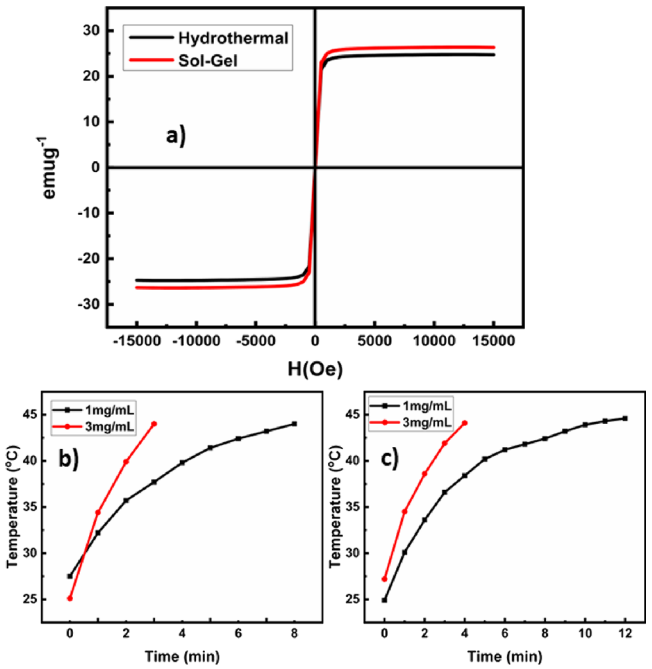


**Figure 3.** (a) Magnetization cycle and (b, c) transient temperature as a function of time of YIG synthesized by the hydrothermal method and sol−gel auto combustion technique.

methods was recorded to measure the surface charge of the prepared samples. The ZP is a function of the surface charge, which develops when any material is placed in a liquid.[39] An increase in the magnitude of the ZP value indicates an increase in the electrostatic repulsion between the particles. The greater the electrostatic repulsion, the stable are the particles. Most of the cellular membranes are negatively charged. ZP has the ability to affect the tendency of NPs to permeate membranes, with cationic particles generally displaying more toxicity associated with cell wall disruption.[40] Low viscosity and high ZP results in the stable and flowable ceramic slurry.[41] The ZP (22.14 mV) of YIG prepared by the hydrothermal technique shows a better colloidal stability compared to sol−gel auto combustion ZP = 18.96 mV.

*3.5.3. Magnetic Hyperthermia.* Magnetic hyperthermia properties of YIG NPs synthesized by hydrothermal and sol−gel auto combustion techniques are studied using an Ambrell EASYHEAT induction system under alternate magnetic fields. Figure 3b,c shows the magnetic hyperthermia property of YIG-synthesized NPs dispersed in hexane at 1 and 3 mg/mL concentrations. The obtained temperature data is plotted as the figure of time period under constant field ($H$) and frequency ($f$).[14] In both the cases, the samples exhibit an increase of the hyperthermia value with YIG concentration under the applied magnetic field parameter. The YIG samples synthesized by both methods have exhibited a steady and nonlinear increase in temperature with respect to time.[18] The heating efficiency of YIG NPs in the presence of an applied magnetic field has been assessed at a 316 kHz constant frequency and a 35.2 $kAm^{-1}$ field strength through estimation of SAR (specific absorption rate), also known as SHGR.[8] The SAR values are calculated using the following relation:[42]

$$\mathrm{SAR} = C_p\left(\frac{dT}{dt}\right)\frac{1}{M_{np}}\mathrm{Js}^{-1}\mathrm{g}^{-1} \quad (1)$$

where $C_p$ is the specific heat capacity of the dispersion medium, $M_{np}$ is the mass of the dispersed samples, and $dT/dt$ is the heating rate. The YIG NPs at various concentrations reached an MH temperature of greater than 43 °C within a short time period, which is an important parameter for MH cancer treatment.[43] The SAR values of YIG at 1 and 3 mg/mL concentrations synthesized by different routes are listed in Table 3. With an increase in the NP concentration, the SAR values are observed to be decreasing. The heat generation capability is dependent on the concentration in two possible ways. The increase in the number of particles increases the number of flips and decreases the interparticle distance.[5] This is due to the interaction of magnetic dipoles with magnetic colloidal particles, leading to a slow magnetic relaxation time.[44] A high SAR value indicates the requirement of less amount of the sample for hyperthermia treatment. This leads to quick biodegradation of NPs in living organs.[14] It is noticed that the particles synthesized using the hydrothermal method produced a lower SAR value than the sol−gel method. Fopase et al. reported the SAR value of YIG particles synthesized by the sol−gel method as 146.76 W/g.[5] In these studies, a higher SAR value is obtained, which is due to the higher saturation magnetization and shorter sintering duration obtained through microwave sintering. However, YIG synthesized by both techniques resulted in good crystallinity with a smaller particle

**Table 3. SAR Values Obtained for YIG at Various Concentrations and Synthesis Techniques**

| synthesis technique | concentration (mg/mL) | SAR ($Js^{-1}$ $g^{-1}$) (~±0.15%) |
|---|---|---|
| hydrothermal | 1 | 214 |
| | 3 | 146 |
| sol−gel auto combustion | 1 | 237 |
| | 3 | 101 |

**Table 2. Comparison of Various Properties of Microwave-Sintered YIG with Literature**

| synthesis technique | sintering method | sintering temperature (°C) | particle size (nm) | $M_s$ ($emug^{-1}$) (~±0.5%) | $M_r$ ($emug^{-1}$) (~±0.5%) | $H_c$ (Oe) (~±0.5%) | reference |
|---|---|---|---|---|---|---|---|
| hydrothermal | microwave | 1250 | 59 | 24.78 | 0.147 | 3.39 | present work |
| sol−gel auto combustion | microwave | 1250 | 56 | 26.39 | 0.145 | 3.14 | present work |
| ball milling | microwave | 1200 | 140 | 16.88 | 1.99 | 48.72 | 37 |
| hydrothermal | conventional | 1100 | 95 | 15.00 | 4.30 | 40.02 | 38 |
| chemical co-precipitation | microwave | 800 | 30 | 29.7 | | 21 | 21 |
| microemulsion | conventional | 1100 | 156 | 19.92 | 18.05 | 7.30 | 36 |



https://doi.org/10.1021/acsomega.3c00162
ACS Omega 2023, 8, 19367−19373

size and a higher magnetic saturation value. Based on this, the samples have achieved a reasonably high SAR value. Hence, the prepared samples are suitable for magnetic hyperthermia cancer applications.

## 4. CONCLUSIONS

In this study, YIG is systematically synthesized by hydrothermal and sol−gel auto combustion methods, followed by microwave sintering. The prepared samples are studied using various characterization techniques. The XRD characterization confirmed the formation of cubic structured YIG, and various structural parameters have been calculated. The morphology of the YIG is studied from SEM images. A comparatively smaller particle size is observed in YIG particles synthesized by the sol−gel auto combustion technique. The optical band gap of the sample is observed to be ∼2.25 eV for both the samples, and the sample is found to be highly transparent near deep UV wavelength. Out of the 25 Raman-active modes, 11 and 12 modes are observed in YIG samples synthesized by hydrothermal and sol−gel auto combustion methods. The garnet phase formation is also confirmed by FTIR studies. The absorption bands are observed in the wavenumber range of 400−800 $cm^{-1}$. A higher saturation magnetization is observed in both the cases compared to other synthesis techniques along with conventional sintering. Compared to the hydrothermal method, YIG NPs synthesized by the sol−gel auto combustion technique give a higher SAR value. The increased SAR value is due to the effective particle size and higher saturation magnetization, which is a suitable candidate for magnetic hyperthermia cancer treatment and other biomedical applications.

## ■ ASSOCIATED CONTENT

### Data Availability Statement

The datasets generated during and/or analyzed during the current study are not publicly available as the data also forms part of the ongoing study but are available from the corresponding author on reasonable request.

### Supporting Information

The Supporting Information is available free of charge at https://pubs.acs.org/doi/10.1021/acsomega.3c00162.

Schematic diagram of the experimental procedure, transmittance graph of the EDAX spectra, and elemental mapping of YIG (PDF)

## ■ AUTHOR INFORMATION


### Corresponding Author

**Madhuri Wuppulluri** − *Ceramic Composites Laboratory, Centre for Functional Materials, Vellore Institute of Technology, Vellore 632014 Tamil Nadu, India;* orcid.org/0000-0002-1650-9931; Email: madhuriw12@hotmail.com

### Authors

**Basil Chacko** − *Department of Physics, School of Advanced Sciences, Vellore Institute of Technology, Vellore 632014 Tamil Nadu, India*

**Avanish Babu Thirumalasetty** − *Department of Physics, School of Advanced Sciences, Vellore Institute of Technology, Vellore 632014 Tamil Nadu, India*

**Vembakam Vijayakanth** − *Center for Nanotechnology Research, Vellore Institute of Technology, Vellore, Tamil Nadu 632014, India*

Complete contact information is available at: https://pubs.acs.org/10.1021/acsomega.3c00162


### Notes

The authors declare no competing financial interest.

## ■ ACKNOWLEDGMENTS

The authors acknowledge SAS, VIT University, for providing XRD, UV, Raman, EDX, SEM, zeta potential, and hyperthermia characterization facilities. We acknowledge the Nanotechnology Research Centre (NRC), SRMIST, for providing the research facilities. No funding has received to carry out this research.

## ■ REFERENCES


(1) Ramesh, T.; Narayana Rao, G.; Suneetha, T.; Shinde, R. S.; Rajendar, V.; Murthy, S. R.; Arun Kumar, S. Microwave-Hydrothermal Synthesis of Y 3 Fe 5 O 12 Nanoparticles : Sintering Temperature Effect on Structural, Magnetic and Dielectric Properties. *J. Supercond. Novel Magn.* **2018**, *31*, 1899−1908.

(2) Hoai Huong, V. T.; Thuy Nguyet, D. T.; Duong, N. P.; Loan, T. T.; Soontaranon, S.; Anh, L. D. Magnetic Interactions and Spin-Wave Stiffness Constant of In-Substituted Yttrium Iron Garnets. *J. Sci. Adv. Mater. Devices* **2020**, *5*, 270−277.

(3) Borade, R. B.; Shirsath, S. E.; Vats, G.; Gaikwad, A. S.; Patange, S. M.; Kadam, S. B.; Kadam, R. H.; Kadam, A. B. Polycrystalline to Preferred-(100) Single Crystal Texture Phase Transformation of Yttrium Iron Garnet Nanoparticles. *Nanoscale Adv.* **2019**, *1*, 403−413.

(4) Shultz, M. D.; Reveles, J. U.; Khanna, S. N.; Carpenter, E. E. Reactive Nature of Dopamine as a Surface Functionalization Agent in Iron Oxide Nanoparticles. *J. Am. Chem. Soc.* **2007**, *129*, 2482−2487.

(5) Fopase, R.; Saxena, V.; Seal, P.; Borah, J. P.; Pandey, L. M. Yttrium Iron Garnet for Hyperthermia Applications: Synthesis, Characterization and in-Vitro Analysis. *Mater. Sci. Eng., C* **2020**, *116*, No. 111163.

(6) Borade, R. B.; Kadam, S. B.; Wagare, D. S.; Kadam, R. H.; Shirsath, S. E.; Nimbore, S. R.; Kadam, A. B. Fabrication of Bi3+ Substituted Yttrium Aluminum Iron Garnet (YAIG) Nanoparticles and Their Structural, Magnetic, Optical and Electrical Investigations. *J. Mater. Sci.: Mater. Electron.* **2019**, *30*, 19782−19791.

(7) Parida, S. C.; Rakshit, S. K.; Singh, Z. Heat Capacities, Order-Disorder Transitions, and Thermodynamic Properties of Rare-Earth Orthoferrites and Rare-Earth Iron Garnets. *J. Solid State Chem.* **2008**, *181*, 101−121.

(8) Manohar, A.; Vijayakanth, V.; Kim, K. H. Influence of Ca Doping on ZnFe2O4 Nanoparticles Magnetic Hyperthermia and Cytotoxicity Study. *J. Alloys Compd.* **2021**, *886*, No. 161276.

(9) Tishin, A. M.; Shtil, A. A.; Pyatakov, A. P.; Zverev, V. I. Developing Antitumor Magnetic Hyperthermia: Principles, Materials and Devices. *Recent Pat. Anti-Cancer Drug Discovery* **2016**, *11*, 360−375.

(10) Pimentel, B.; Caraballo-Vivas, R. J.; Checca, N. R.; Zverev, V. I.; Salakhova, R. T.; Makarova, L. A.; Pyatakov, A. P.; Perov, N. S.; Tishin, A. M.; Shtil, A. A.; Rossi, A. L.; Reis, M. S. Threshold Heating Temperature for Magnetic Hyperthermia: Controlling the Heat Exchange with the Blocking Temperature of Magnetic Nanoparticles. *J. Solid State Chem.* **2018**, *260*, 34−38.

(11) Gillooly, J. F.; Brown, J. H.; West, G. B.; Savage, V. M.; Charnov, E. L. Effects of Size and Temperature on Metabolic Rate. *Science* **2001**, *293*, 2248−2251.

(12) Dill, K. A.; Ghosh, K.; Schmit, J. D. Physical Limits of Cells and Proteomes. *Proc. Natl. Acad. Sci. U. S. A.* **2011**, *108*, 17876−17882.

(13) Ritchie, M. E. Reaction and Diffusion Thermodynamics Explain Optimal Temperatures of Biochemical Reactions. *Sci. Rep.* **2018**, *8*, 1−10.
(14) Vijayakanth, V.; Vinodhini, V.; Aparna, A.; Malavika, M. S.; Krishnamoorthi, C. Synthesis and Magnetic Hyperthermia Properties of Zwitterionic Dopamine Sulfonate Ligated Magnesium Ferrite and Zinc Ferrite Nanoparticles. *J. Mater. Sci.: Mater. Electron.* **2021**, *32*, 2395−2408.
(15) Van der Zee, J. Heating the Patient: A Promising Approach? *Ann. Oncol.* **2002**, *13*, 1173−1184.
(16) Wust, P.; Hildebrandt, B.; Sreenivasa, G.; Rau, B.; Gellermann, J.; Riess, H.; Felix, R.; Schlag, P. M. Hyperthermia in Combined Treatment of Cancer. *Lancet Oncol.* **2002**, *3*, 487−497.
(17) Roizin-Towle, L.; Pirro, J. P. The Response of Human and Rodent Cells to Hyperthermia. *Int. J. Radiat. Oncol., Biol., Phys.* **1991**, *20*, 751−756.
(18) Vijayakanth, V.; Krishnamoorthi, C. Effect of Zwitterionic Surfactant Ligand Monolayer on Magnetic Hyperthermia Properties of Monosize Fe3O4 Nanoparticles. *J. Supercond. Novel Magn.* **2021**, *34*, 623−632.
(19) Shirsath, S. E.; Wang, D.; Jadhav, S. S.; Mane, M. L.; Li, S. *Ferrites Obtained by Sol-Gel Method*; Springer, 2018, DOI: 10.1007/978-3-319-32101-1_125.
(20) Naidu, K. C. B.; Madhuri, W. Hydrothermal Synthesis of NiFe2O4 Nano-Particles: Structural, Morphological, Optical, Electrical and Magnetic Properties. *Bull. Mater. Sci.* **2017**, *40*, 417−425.
(21) Liu, J.; Yu, P.; Jin, Q.; Zhang, C.; Zhang, M.; Harris, V. G. Microwave-Accelerated Rapid Synthesis of High-Quality Yttrium Iron Garnet Nano Powders with Improved Magnetic Properties. *Mater. Res. Lett.* **2018**, *6*, 36−40.
(22) Sharma, V.; Saha, J.; Patnaik, S.; Kuanr, B. K. Synthesis and Characterization of Yttrium Iron Garnet (YIG) Nanoparticles - Microwave Material. *AIP Adv.* **2017**, *7*, No. 056405.
(23) Patterson, A. L. The Scherrer Formula for X-Ray Particle Size Determination. *Phys. Rev.* **1939**, *56*, 978−982.
(24) Somvanshi, S. B.; Patade, S. R.; Andhare, D. D.; Jadhav, S. A.; Khedkar, M. V.; Kharat, P. B.; Khirade, P. P.; Jadhav, K. M. Hyperthermic Evaluation of Oleic Acid Coated Nano-Spinel Magnesium Ferrite: Enhancement via Hydrophobic-to-Hydrophilic Surface Transformation. *J. Alloys Compd.* **2020**, *835*, No. 155422.
(25) Chacko, B.; Roy, A.; Melbin Richard, A.; Swathy, J.; Avanish, B. T.; Madhuri, W. Bismuth Modified Zinc Ferrites for Low-Temperature Ceramic Co-Firing Technology. *Mater. Chem. Phys.* **2022**, *276*, No. 125401.
(26) Syazwan Mustaffa, M.; Hashim, M.; Azis, R. S.; Ismail, I.; Kanagesan, S.; Misbah Zulkimi, M. Magnetic Phase-Transition Dependence on Nano-to-Micron Grain-Size Microstructural Changes of Mechanically Alloyed and Sintered Ni0.6Zn0.4Fe2 O 4. *J. Supercond. Novel Magn.* **2014**, *27*, 1451−1462.
(27) Khan, M. S. I.; Oh, S. W.; Kim, Y. J. Power of Scanning Electron Microscopy and Energy Dispersive X-Ray Analysis in Rapid Microbial Detection and Identification at the Single Cell Level. *Sci. Rep.* **2020**, *10*, 1−10.
(28) Tauc, J.; Grigorovici, R.; Vancu, A. Optical Properties and Electronic Structure of Amorphous Germanium. *Phys. Status Solidi* **1966**, *15*, 627−637.
(29) Monteseguro, V.; Rodríguez-Hernández, P.; Vilaplana, R.; Manjón, F. J.; Venkatramu, V.; Errandonea, D.; Lavín, V.; Muñoz, A. Lattice Dynamics Study of Nanocrystalline Yttrium Gallium Garnet at High Pressure. *J. Phys. Chem. C* **2014**, *118*, 13177−13185.
(30) Barrón-López, J. F.; Hernández-Cruz, L. E.; Sánchez De-Jesús, F.; Bolarín-Miró, A.; Alvarez, G.; Montiel, H. Vibrational and Magnetic Properties of YIG Ferrite Powders Obtained by the Pechini Method. *J. Phys. Conf. Ser.* **2019**, *1221*, No. 012017.
(31) Peña-Garcia, R.; Delgado, A.; Guerra, Y.; Duarte, G.; Gonçalves, L. A. P.; Padrón-Hernández, E. The Synthesis of Single-Phase Yttrium Iron Garnet Doped Zinc and Some Structural and Magnetic Properties. *Mater. Res. Express* **2017**, *4*, No. 016103.
(32) Fechine, P. B. A.; Silva, E. N.; Menezes, A. S.; Derov, J.; Stewart, J. W.; Drehman, A. J.; Vasconcelos, I. F.; Ayala, A. P.; Cardoso, L. P.; Sombra, A. S. B. Journal of Physics and Chemistry of Solids Synthesis, Structure and Vibrational Properties of GdIG X : YIG 1 À X Ferrimagnetic Ceramic Composite. *J. Phys. Chem. Solids* **2009**, *70*, 202−209.
(33) Condon, E. A Theory of Intensity Distribution in Band Systems. *Phys. Rev.* **1926**, *28*, 1182−1201.
(34) Paiva, D. V. M.; Silva, M. A. S.; Ribeiro, T. S.; Vasconcelos, I. F.; Sombra, A. S. B.; Góes, J. C.; Fechine, P. B. A. Novel Magnetic − Dielectric Composite Ceramic Obtained from Y 3 Fe 5 O 12. *J. Alloys Compd.* **2015**, *644*, 763−769.
(35) Monteseguro, V.; Rodríguez-Hernández, P.; Ortiz, H.; Venkatramu, V.; Manjón, F. J.; Jayasankar, C.; Lavín, V.; Muñoz, A. Structural, Elastic and Vibrational Properties of Nanocrystalline Lutetium Gallium Garnet under High Pressure. *Phys. Chem. Chem. Phys.* **2015**, *17*, 9454−9464.
(36) Akhtar, M. N.; Bakar Sulong, A.; Khan, M. A.; Ahmad, M.; Murtaza, G.; Raza, M. R.; Raza, R.; Saleem, M.; Kashif, M. Structural and Magnetic Properties of Yttrium Iron Garnet (YIG) and Yttrium Aluminum Iron Garnet (YAIG) Nanoferrites Prepared by Micro-emulsion Method. *J. Magn. Magn. Mater.* **2016**, *401*, 425−431.
(37) Khade, V.; Heena, S.; Nayak, A.; Sharanya, H.; Sahana, C. S.; Parhi, C. C.; Wuppulluri, M. Structural And Magnetic Characteristics Of Microwave Sintered Yttrium Iron Garnet ( YIG ). *Solid State Technol.* **2020**, *63*, 7824−7830.
(38) Mansournia, M.; Orae, M. Yttrium-Iron Garnet and Yttrium Orthoferrite Nanocrystals: Hydrothermal Synthesis, Magnetic Property and Phase Transformation Study. *J. Rare Earths* **2018**, *36*, 1292−1298.
(39) Weiner, B. B.; Tscharnuter, W. W.; Fairhurst, D.; Instruments, B.; Holtsville, C.; Us, N. Y.; Weiner, B. B.; Tscharnuter, W. W. Zeta Potential : By A New Approach. In *Canadian Mineral Analysts Meeting*; Brookhaven Instruments Corporation: Winnipeg Canada, 1993.
(40) Clogston, J. D.; Patri, A. K. Zeta Potential Measurement. *Methods Mol. Biol.* **2011**, *697*, 63−70.
(41) Xu, W.; Yang, J.; Jin, Y.; Qiu, T. Aqueous Gelcasting of Yttrium Iron Garnet. *J. Eur. Ceram. Soc.* **2013**, *33*, 1023−1028.
(42) Manohar, A.; Vijayakanth, V.; Pallavolu, M. R.; Kim, K. H. Effects of Ni - Substitution on Structural, Magnetic Hyperthermia, Photocatalytic and Cytotoxicity Study of MgFe2O4 Nanoparticles. *J. Alloys Compd.* **2021**, *879*, No. 160515.
(43) Shah, S. A.; Asdi, M. H.; Hashmi, M. U.; Umar, M. F.; Awan, S.-U. Thermo-Responsive Copolymer Coated MnFe2O4 Magnetic Nanoparticles for Hyperthermia Therapy and Controlled Drug Delivery. *Mater. Chem. Phys.* **2012**, *137*, 365−371.
(44) Manohar, A.; Krishnamoorthi, C.; Naidu, K. C. B.; Pavithra, C. Dielectric, Magnetic Hyperthermia, and Photocatalytic Properties of ZnFe2O4 Nanoparticles Synthesized by Solvothermal Reflux Method. *Appl. Phys. A: Mater. Sci. Process.* **2019**, *125*, 477.


https://doi.org/10.1021/acsomega.3c00162
*ACS Omega* 2023, 8, 19367−19373